Journal of Computational Physics: X 8 (2020) 100079

Contents lists available at ScienceDirect

Journal of Computational Physics: X

www.elsevier.com/locate/jcpx

Two-dimensional leapfrog scheme for trajectories of relativistic charged particles in static axisymmetric electric and magnetic field

Chuanren Wu *, Ioannis Gr. Pagonakis, Stefan Illy, John Jelonnek

Karlsruhe Institute of Technology (KIT), Institute for Pulsed Power and Microwave Technology (IHM), 76344 Eggenstein-Leopoldshafen, Germany

ARTICLE INFO

Article history:
Received 7 August 2019
Received in revised form 12 October 2020
Accepted 15 October 2020
Available online 16 October 2020

Keywords:
Charged particle beams
Vacuum tubes
Gyrotrons
Gyro-TWTs
Electron guns
Collectors

ABSTRACT

A method for the calculation of two-dimensional particle trajectories is proposed in this work. It makes use of the cylindrical symmetry and the simplification of the static electric field, so that there should be no systematic error for the centered large-orbit rotations nor for the acceleration or deceleration in a uniform electric field. The method also shows a lower error level than the standard Boris method in many cases. Typical applications of this method are for example, electron microscopes, electron guns and collectors of gyro-devices as well as of other vacuum tubes, which can be described in axisymmetric cylindrical coordinates. Besides, the proposed method enforces the conservation of canonical angular momentum by construction, which is expected to show its advantages in the simulation of cusp electron guns and other components relying on non-adiabatic transitions in the externally applied static magnetic field.

1. Introduction

Gyrotron oscillators are vacuum tubes, which are used as sources for the RF heating and current drive in the magnetically confined nuclear fusion experiments [1], and for the dynamic nuclear polarization in the NMR spectroscopy [2]. Amplifiers like gyro-TWTs and gyro-klystrons can be applied, for example, in the W-band radars [3]. The full-wave simulation of a gyro-device as a whole tube is impractical due to the requirement of the computational resources. Therefore, the components of a gyro-device are typically simulated separately, where different simplifications are considered for different types of components. For instance,

- There are special codes e.g. [4,5] for the simulation of the interaction between RF wave and electron beam using advanced models. These codes model the physics clearer than a numerical black box and can simulate the interactions within a reasonable time.
- The code for the simulation of the RF output system does not need to consider the interaction with particles.
- The simulation of electron guns and collectors does not need to include the interaction with the RF waves.

* Corresponding author.
E-mail address: chuanren.wu@kit.edu (C. Wu).

https://doi.org/10.1016/j.jcpx.2020.100079

Nomenclature

γ	Lorentz factor	c	speed of light
φ	electric potential	g	a position-dependent scalar
θ	the azimuthal angular coordinate	m_0	rest mass of a particle
Δt	time step	q	charge of a particle (negative for electrons)
$\mathcal{E}_{\text{kin}}$	kinetic energy of a particle	$\boldsymbol{A}$	magnetic vector potential
$\mathcal{E}_{\text{total}}$	total energy of a particle	$\boldsymbol{x}$	coordinates (z, r) of a particle
P_θ	canonical angular momentum	$\boldsymbol{u}$	product of γ and velocity $\boldsymbol{v}$
$[\cdot]_t$	the value of a variable at discrete time t		

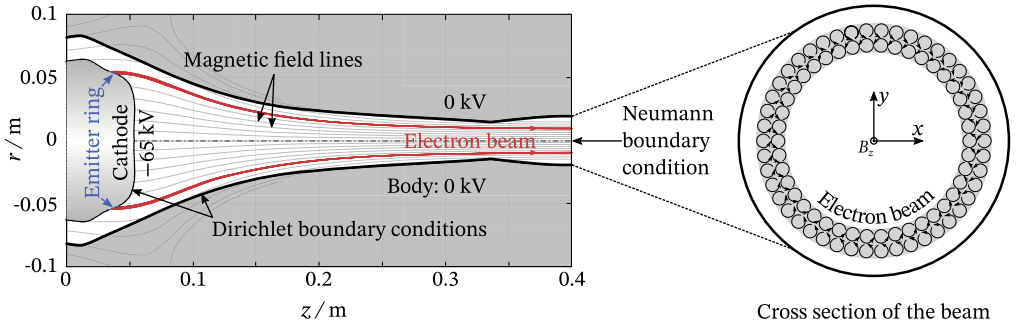

Fig. 1. Electron gun for gyrotron.

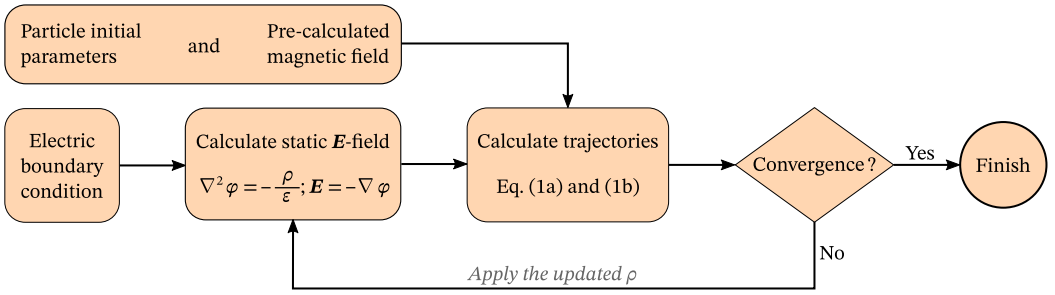

Fig. 2. Calculation of electron guns and collectors.

The code for the last point is the topic of this work. In the electron guns and collectors there are numerous electrons, whose trajectories need to be traced and resolved accurately in the static fields. It is necessary to improve the calculation of the trajectories, in order to optimize the speed and accuracy of the simulations.

The electron guns and collectors of gyro-devices can be usually modeled and simulated in cylindrical coordinates. An example of a small-orbit gyrotron electron gun (so-called *magnetron injection gun*) is given in Fig. 1. Electrons are emitted from the emitter ring with a negative potential and are accelerated by the electric field. There is a set of coils (outside the range of the figure) creating an increasing magnetic field, which compresses the annular electron beam and guides the beam towards the RF cavity. On the right-hand side of the figure, the cross section of such an annular electron beam is shown qualitatively. The gyration of the electrons should be accurately resolved in the simulations. The outputs of the simulation are the positions and the velocity components of the beam electrons.

The transient process in the electron guns and collectors is usually not needed (but can also be considered with the proposed method, via adjusting the total energy), instead, the final stationary state is going to be solved. The stationary state can be obtained by the process as shown in Fig. 2. In the following text, an electron beam is chosen for the explanation; however, the process can be applied to other charged particles including a mixture of various species. As it is not always possible to track every real particle due to the large quantity, a “macro particle” will represent a group of the same kind of physical particles in the numerical simulations. Since the m_0/q ratio of a macro particle and a physical particle are identical, the macro one and the physical particle leave the same trajectory. Therefore, the terms “an electron” and “a particle” will be used in the following text.

As shown in Fig. 2. First, the magnetic field in the simulation region is solved by Biot-Savart integrals over all coil currents or by other appropriate methods e.g. the finite element method. The initial electric field, when the electron beam is absent, is solved for the given electric boundary conditions (see Fig. 1). Then, the electrons are injected and pushed

individually. At this stage, an electron is not aware of other electrons in the space. After all macro electrons in the electron beam are processed, a new distribution of the charge density ρ will be calculated, which also includes the space charges of the electron beam from the previous iteration. With the new electric field calculated from the updated charge density function, trajectories of the beam electrons will be calculated once again, so on and so forth. The convergence is a necessary condition for a reliable design of the devices. Otherwise, it indicates that the electron beam might interact with its space charge unstably. Optionally, the magnetic field induced by the electron beam can also be considered in each iteration; however, this field is safely negligible compared to the magnetic field from the coils for most cases.

The process in Fig. 2 involves only static electric and magnetic field, though the fields vary between iterations. In addition, the classical designs of the components are axisymmetric, such that the fields and geometries are possible to be described in two dimensions. When the system is axisymmetric, the canonical angular momentum is conserved, which is also known as Busch's theorem [6]. Various codes have been designed for the simulation of the electron guns and collectors such as EGUN [7], BFCPIC [8], DAPHNE [9], CIELAS [10], and EPOS [11]. At KIT, the codes ESRAY [12] and ARIADNE [13] are used. Both codes have been designed to consider the cylindrical coordinates and the symmetric static fields. However, in order to make a better use of this special situation, one could also consider the kinetic energy to be only position-dependent (as the electric field is free of rotation) and the conservation of the canonical angular momentum, which are hard to be taken into account using the existing methods for the particle dynamics.

Two methods: Boris and the classical 4th-order Runge-Kutta were implemented in the code ESRAY and ARIADNE. Boris algorithm [14] is time-reversible [15] and volume preserving in phase space [16]. It has been widely applied and well studied for plasma [17] and accelerator [18,19] simulations, which is not only suitable for such static field scenarios but can also include the interaction with RF waves. Several variants of Boris algorithm are compared in [20]. In particular, improvements based on Boris method have been reported [21–23], for a better accuracy of relativistic particle motions, rotation resolution and preserving the $\boldsymbol{E}\times\boldsymbol{B}$ drift. Beyond the standard two-step Boris method, the three-step variant [24] can improve the accuracy for $\omega_c\,\Delta t > 1$ [25], while the accuracy can be further improved by using more sub-steps [26,27]. There are also methods considering cylindrical coordinates [28,29]. A (non-relativistic) formulation [30] derived from the Hamiltonian preserves the energy exactly. However, the special properties (2D axisymmetric, angular momentum conservation, electrostatic) of targeted applications were not fully utilized in the existing methods.

The method proposed in this work considers the conservations of energy and canonical angular momentum. A two-dimensional leapfrog algorithm is proposed based on the equations, but the extension to a higher order is also possible. The formulation and the steps of implementation are explained in section 2. Comparisons to the standard Boris and Runge-Kutta method are presented in section 3.

2. Formulation and implementation of the proposed method

2.1. Formulation of the two-dimensional method

During one iteration in the loop of Fig. 2, the axisymmetric $\boldsymbol{E}(z,r)$ field was pre-calculated from the Poisson equation and $\boldsymbol{B}(z,r)$ was calculated from the external coils. They do not vary during the calculation of particle motions. The position $\boldsymbol{x}$ of a charged particle is updated by

$$\frac{\mathrm{d}\boldsymbol{x}}{\mathrm{d}t} = \boldsymbol{v} \quad \text{where} \quad \boldsymbol{v} = \frac{\boldsymbol{u}}{\gamma}\,. \tag{1a}$$

The acceleration only considers Lorentz force

$$m_0\,\frac{\mathrm{d}\boldsymbol{u}}{\mathrm{d}t} = q\left(\boldsymbol{E} + \boldsymbol{v}\times\boldsymbol{B}\right), \tag{1b}$$

where m_0 and q are constants of a particle. The general form of $\mathrm{d}\boldsymbol{u}/\mathrm{d}t$ in cylindrical coordinates (z,r,θ) can be found in textbooks (e.g. chapter 2.1 of [31]). Here, it is practical to assume

$$\left|\,B_\theta\,/\,B_{\text{total}}\,\right| \ll 1 \;\text{ or even }\; B_\theta = 0\,, \tag{2}$$

since considering a nonzero B_θ component does not affect the simulation results for the targeted applications. For example, the maximum $B_\theta/B_{\text{total}}$ ratio from the quasi-optical launcher until the end of collector in the ITER gyrotron [32] with 45 A electron beam current, is in the order of 1×10^{-6}, according to simulations. Everywhere else, $B_\theta/B_{\text{total}}$ is significantly lower than that maximum. Applying eq. (2) to eq. (1b), the time derivative of $\boldsymbol{u}$ on the (z,r) plane is

$$\frac{\mathrm{d}\boldsymbol{u}}{\mathrm{d}t} = \begin{pmatrix} \dfrac{q}{m_0}\left(E_z - v_\theta\,B_r\right) \\[2ex] \dfrac{q}{m_0}\,E_r + v_\theta\left(\dfrac{u_\theta}{r} + \dfrac{q}{m_0}\,B_z\right) \end{pmatrix}. \tag{3}$$

From now on, the notations of vectors and their operations are in the two-dimensional (z,r) projection, i.e. $\boldsymbol{u} = (u_z, u_r)$ and $\nabla = (\partial/\partial z, \partial/\partial r)$.

Two conservations can be utilized for the evaluation of eq. (3). One conserved quantity is the canonical angular momentum

$$P_\theta = m_0\, r\, u_\theta + q\, r\, A_\theta = \text{const.} \tag{4a}$$

of each particle in the axisymmetric system. Therefore, u_θ in eq. (3) is evaluated as

$$u_\theta(z,r) = \frac{P_\theta}{m_0\, r} - \frac{q}{m_0}\, A_\theta(z,r)\ . \tag{4b}$$

Another conserved quantity is the total energy of a particle in the electrostatic field

$$\mathcal{E}_{\text{total}} = \mathcal{E}_{\text{kin}} + q\,\varphi(z,r) = \text{const.} \tag{5a}$$

The Lorentz factor can be written as a function only of position

$$\gamma(z,r) = 1 + \frac{\mathcal{E}_{\text{kin}}}{m_0\, c^2} = 1 + \frac{\mathcal{E}_{\text{total}} - q\,\varphi(z,r)}{m_0\, c^2}\ . \tag{5b}$$

Consequently, the velocity component

$$v_\theta(z,r) = \frac{u_\theta(z,r)}{\gamma(z,r)} \tag{5c}$$

depends only on position, too. Inserting eqs. (4b) and (5c) into eq. (3), the right-hand side of eq. (3) also becomes a function only of particle position. In this way, the two-dimensional Lorentz force is decoupled from the particle velocity.

An alternative formulation only using A_θ and φ is given in eq. (A.7). In addition, one can define an effective scalar potential field. However, the classical effective potential (e.g. in chapter 2.6 of [33]) is not suitable for the calculation of relativistic particle trajectories. In this context, a position-dependent potential g can be derived, see eq. (A.2).

2.2. Implementation of the method

In the numerical implementation, each particle has, during its whole "life time", four constants $\mathcal{E}_{\text{total}}$, P_θ, q and m_0, whereas the state of a particle consists of two vectors $\boldsymbol{x} = (z, r)$ and $\boldsymbol{u} = (u_z, u_r)$. The leapfrog algorithm with staggered $\boldsymbol{x}$ and $\boldsymbol{u}$ is applied here to advance the state of particles for its simplicity (other methods are also possible). The outputs of each step are $[\boldsymbol{u}]_{t_0+\frac{1}{2}\Delta t}$ and $[\boldsymbol{x}]_{t_0+\Delta t}$.

First, it is straightforward to advance the velocity $\boldsymbol{u}$ according to eq. (3):

$$\frac{[\boldsymbol{u}]_{t_0+\frac{1}{2}\Delta t} - [\boldsymbol{u}]_{t_0-\frac{1}{2}\Delta t}}{\Delta t} = \left(\begin{array}{c} \dfrac{q}{m_0}\,(E_z - v_\theta\, B_r) \\ \dfrac{q}{m_0}\, E_r + v_\theta \left(\dfrac{u_\theta}{r} + \dfrac{q}{m_0}\, B_z \right) \end{array} \right)_{\text{at time } t_0} \tag{6a}$$

or equivalently, the (A, ϕ) formulation from eq. (A.7) can be implemented as

$$\frac{[\boldsymbol{u}]_{t_0+\frac{1}{2}\Delta t} - [\boldsymbol{u}]_{t_0-\frac{1}{2}\Delta t}}{\Delta t} = \left(\begin{array}{c} \dfrac{q}{m_0} \left(v_\theta\, \dfrac{\partial A_\theta}{\partial z} - \dfrac{\partial \varphi}{\partial z} \right) \\ \dfrac{v_\theta\, P_\theta}{m_0\, r^2} + \dfrac{q}{m_0} \left(v_\theta\, \dfrac{\partial A_\theta}{\partial r} - \dfrac{\partial \varphi}{\partial r} \right) \end{array} \right)_{\text{at time } t_0}\ . \tag{6b}$$

Every variable on the right-hand side of eq. (6) is known at time t_0.

Then, the position will be updated by

$$\frac{[\boldsymbol{x}]_{t_0+\Delta t} - [\boldsymbol{x}]_{t_0}}{\Delta t} = \frac{[\boldsymbol{u}]_{t_0+\frac{1}{2}\Delta t}}{[\gamma]_{t_0+\frac{1}{2}\Delta t}}\ . \tag{7}$$

However, γ at time $t_0 + \frac{1}{2}\Delta t$ is unknown. The Lorentz factor γ is a function only of $\boldsymbol{x}$ in each iteration of Fig. 2. It is known at time t_0. Based on the value at time t_0, a series of γ can be expanded:

$$[\gamma]_{t_0+\frac{1}{2}\Delta t} \approx [\gamma]_{t_0} + [\nabla\gamma]_{t_0} \cdot \frac{[\boldsymbol{u}]_{t_0+\frac{1}{2}\Delta t}}{[\gamma]_{t_0+\frac{1}{2}\Delta t}}\ \frac{\Delta t}{2}\ , \tag{8}$$

where $[\nabla\gamma]_{t_0}$ is

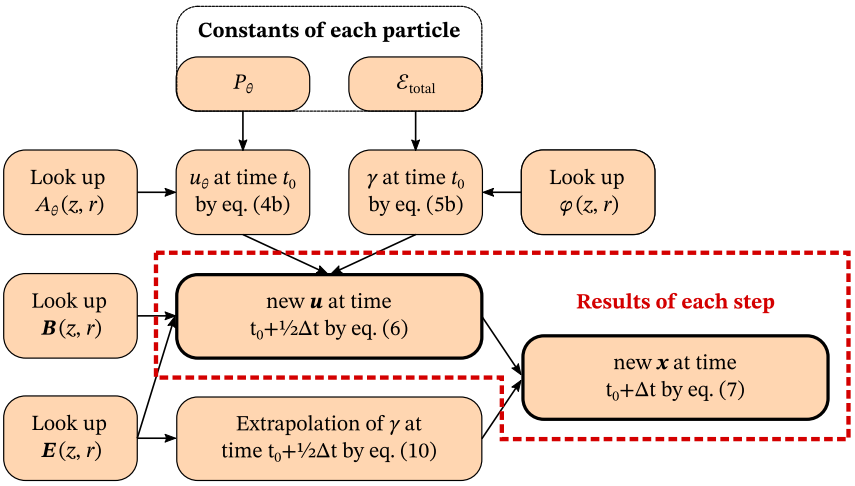

Fig. 3. One step of the two-dimensional leapfrog method.

$$\nabla\gamma = \frac{\mathrm{d}\,\gamma}{\mathrm{d}\,\varphi}\,\nabla\varphi = -\frac{q}{m_0\,c^2}\,\nabla\varphi = \frac{q}{m_0\,c^2}\,\boldsymbol{E}\,, \tag{9}$$

at the position $[\boldsymbol{x}]_{t_0}$. Equation (8) has two roots:

$$[\gamma]_{t_0+\frac{1}{2}\Delta t} = \frac{1}{2}\left([\gamma]_{t_0} \pm \sqrt{[\gamma]_{t_0}^2 + \frac{2\,q}{m_0\,c^2}\,\Delta t\,\left\{[\boldsymbol{u}]_{t_0+\frac{1}{2}\Delta t}\cdot\boldsymbol{E}([\boldsymbol{x}]_{t_0})\right\}}\right)\,. \tag{10}$$

Only the upper (+) root is acceptable, as the lower (−) one would lead to $\gamma \to 0$, which is not physical. This is a highlight of the proposed method. It is proven in appendix B that in absence of magnetic field, this method yields the exact trajectory in a constant electric field, while in a linearly varying electric field, the accuracy of trajectories is also significantly (e.g. 12000 times) better than the standard Boris method for the same order of convergence. Detailed comparisons can be found in section 3.1.

From a pure physics point of view, the mesh grid only has to store $\boldsymbol{A}$ and φ. Equation (6b) is evaluated to advance the velocity. This requires the derivations of potentials. Another possibility is to store all $(\boldsymbol{E}, \varphi, \boldsymbol{B}, A_\theta)$ values in the same or different grids. Depending on the applied numerical method for the calculation of fields, numerical derivatives could be avoided, especially when a low-order interpolation of fields is considered. An example is elaborated in the next paragraph.

For the applications described in section 1, typically, both $\boldsymbol{B}$ and A_θ can be calculated from the integrals of coil currents. They are calculated only once, during the initialization. Since no derivative will be evaluated, $\boldsymbol{B}$ and A_θ can be stored in the same uniform grid independent of the shape of electric boundaries. Mapping the coordinates of a particle to the cell location in the uniform grid is fast and straightforward. Not much effort will be added, when A_θ is stored and interpolated alongside $\boldsymbol{B}$. For the finite element or finite difference methods, the $\boldsymbol{E}$ field in a mesh cell is derived from φ; whereas in particular formulations of boundary element method, $\boldsymbol{E}$ on the grid can be integrated from the charge densities in each iteration without numerical derivatives. Moreover, local mesh grids [34] can be applied to improve the performance. A graphical overview of the calculation steps using all of the field quantities $(\boldsymbol{E}, \varphi, \boldsymbol{B}, \boldsymbol{A})$ is depicted in Fig. 3.

3. Comparison to the other methods in various scenarios

The proposed method will be compared to the standard Boris and the 4th-order Runge-Kutta method using concrete examples. Their implementations are explained as follows:

- The proposed method needs the implementations of eqs. (4b), (5b), (6a), (7) and (10). Totally six field scalars B_z, B_r, A_θ, E_z, E_r, and φ are fetched once at the point $[\boldsymbol{x}]_{t_0}$ in each time step. Here, the fields will be given analytically. In case of using mesh grids, the components of B and A_θ can be stored in a uniform mesh grid or share the grid with the E field, while ϕ and the components of E can share a grid. This method is expected to have a second-order convergence for one force evaluation per time step.
- Boris method is implemented according to chapter 15 of [17]. The vectors $\boldsymbol{u}$ and $\boldsymbol{x}$ are staggered in time. The equations for the transition from the current state $\left([\boldsymbol{x}]_{t_0}, [\boldsymbol{u}]_{t_0-\frac{1}{2}\Delta t}\right)$ to the next state $\left([\boldsymbol{x}]_{t_0+\Delta t}, [\boldsymbol{u}]_{t_0+\frac{1}{2}\Delta t}\right)$ are

$$\boldsymbol{u}_- = [\boldsymbol{u}]_{t_0-\frac{1}{2}\Delta t} + \frac{q\,\Delta t}{2\,m_0}\,\boldsymbol{E}([\boldsymbol{x}]_{t_0}) \tag{11a}$$

$$\boldsymbol{u}_+ = \boldsymbol{u}_- + \frac{2}{1+s^2}\,(\boldsymbol{u}_- + \boldsymbol{u}_- \times \boldsymbol{s}) \times \boldsymbol{s} \quad \text{where} \quad \boldsymbol{s} = \frac{q\,\Delta t}{2\,\gamma\, m_0}\,\boldsymbol{B}([\boldsymbol{x}]_{t_0}) \quad \text{with} \quad \gamma = \sqrt{1+\frac{(u_-)^2}{c^2}} \tag{11b}$$

$$[\boldsymbol{u}]_{t_0+\frac{1}{2}\Delta t} = \boldsymbol{u}_+ + \frac{q\,\Delta t}{2\,m_0}\,\boldsymbol{E}([\boldsymbol{x}]_{t_0}) \tag{11c}$$

$$[\boldsymbol{x}]_{t_0+\Delta t} = [\boldsymbol{x}]_{t_0} + \frac{[\boldsymbol{u}]_{t_0+\frac{1}{2}\Delta t}}{[\gamma]_{t_0+\frac{1}{2}\Delta t}}\,\Delta t \quad \text{where} \quad [\gamma]_{t_0+\frac{1}{2}\Delta t} = \sqrt{1+\left([u]_{t_0+\frac{1}{2}\Delta t}/c\right)^2} \tag{11d}$$

The fields (B_x, B_y, B_z) and (E_x, E_y, E_z) at point $[\boldsymbol{x}]_{t_0}$ are fetched once per time step. Boris method has second-order convergence. If the field components are considered as scalars, the number of scalars to be interpolated from the grid is the same as the proposed method.

- In the classical 3D Runge-Kutta method (RK4), the position and velocity of a particle is given at the same time. To simplify the formulation, a function $\mathcal{H}$ is defined as

$$\mathcal{H}\begin{pmatrix}\boldsymbol{x}\\ \boldsymbol{u}\end{pmatrix} := \begin{pmatrix}\boldsymbol{v}\\ \frac{q}{m_0}\Big[\boldsymbol{E}(\boldsymbol{x}) + \boldsymbol{v}\times\boldsymbol{B}(\boldsymbol{x})\Big]\end{pmatrix}\Delta t \quad \text{where} \quad \boldsymbol{v} = \frac{\boldsymbol{u}}{\sqrt{1+u^2/c^2}} \tag{12a}$$

and the previous state of a step is written as

$$[\boldsymbol{X}]_{t_0} := \begin{pmatrix}[\boldsymbol{x}]_{t_0}\\ [\boldsymbol{u}]_{t_0}\end{pmatrix}. \tag{12b}$$

The implementation of RK4 can be formulated using $\mathcal{H}$ as

$$\boldsymbol{h}_1 = \mathcal{H}\Big([\boldsymbol{X}]_{t_0}\Big) \quad ; \quad \boldsymbol{h}_2 = \mathcal{H}\left([\boldsymbol{X}]_{t_0} + \frac{\boldsymbol{h}_1}{2}\right) \quad ; \quad \boldsymbol{h}_3 = \mathcal{H}\left([\boldsymbol{X}]_{t_0} + \frac{\boldsymbol{h}_2}{2}\right) \quad ; \quad \boldsymbol{h}_4 = \mathcal{H}\Big([\boldsymbol{X}]_{t_0} + \boldsymbol{h}_3\Big) \tag{12c}$$

$$[\boldsymbol{X}]_{t_0+\Delta t} = \begin{pmatrix}[\boldsymbol{x}]_{t_0+\Delta t}\\ [\boldsymbol{u}]_{t_0+\Delta t}\end{pmatrix} = [\boldsymbol{X}]_{t_0} + \frac{1}{6}\,(\boldsymbol{h}_1 + 2\,\boldsymbol{h}_2 + 2\,\boldsymbol{h}_3 + \boldsymbol{h}_4)\,. \tag{12d}$$

The function $\mathcal{H}$ has to be evaluated at four different points per time step. The field components at these four points need to be interpolated, while the number of scalar field components to be interpolated at each point is the same as the other two methods. Therefore, RK4 is expected to take 4 times calculation time as the other two methods. Although RK4 costs significantly more time to calculate, it has 4th-order convergence and can use an adaptive Δt.

The comparisons only consider a single probe electron in a single iteration of Fig. 2, where the applied electric and magnetic field are defined by elementary functions, in order to exclude the error of field interpolations. Besides, exact analytical solutions can be derived from the analytical field functions in certain scenarios. The fields are given in the two-dimensional (z, r) coordinates for all three cases, while the states $(\boldsymbol{x}, \boldsymbol{u})$ of the particles in RK4 and Boris method are in 3D Cartesian coordinates.

3.1. Acceleration by an electric field

The error of the acceleration or deceleration by electric field will be checked in this section. In particular, the following three scenarios will be considered:

- The basic scenario: a uniform constant axial electric field $E(z) = E_z$ without magnetic field.
- Including the first-order term of the axial electric field: $E(z) = E_z + z\,E_z'$ without magnetic field.
- Including a perpendicular magnetic field: $E(z) = E_z$ with a constant B_r component of magnetic field. (B_z will be considered in the next sections.)

The error of final axial positions for the same total travel time (16 ps) will be compared. The reasons for choosing these scenarios are the follows. The first scenario has an analytical solution. It will be shown that the proposed method yields the exact solution for this field. However, if the electric field strength has a gradient, the assumptions for the exact solution are broken; therefore, the second scenario is introduced to check the error in such an electric field. On the other hand, introducing a magnetic field breaks the assumptions of the exact solution, too. This is the third scenario. When the particle starts to move axially like in the first case, the magnetic field component B_r exerts a force in θ direction, which causes the probe electron to gyrate. The gyration exerts then another axial force. The system becomes complicated and the reference result z_{expect} of this scenario has to be calculated numerically.

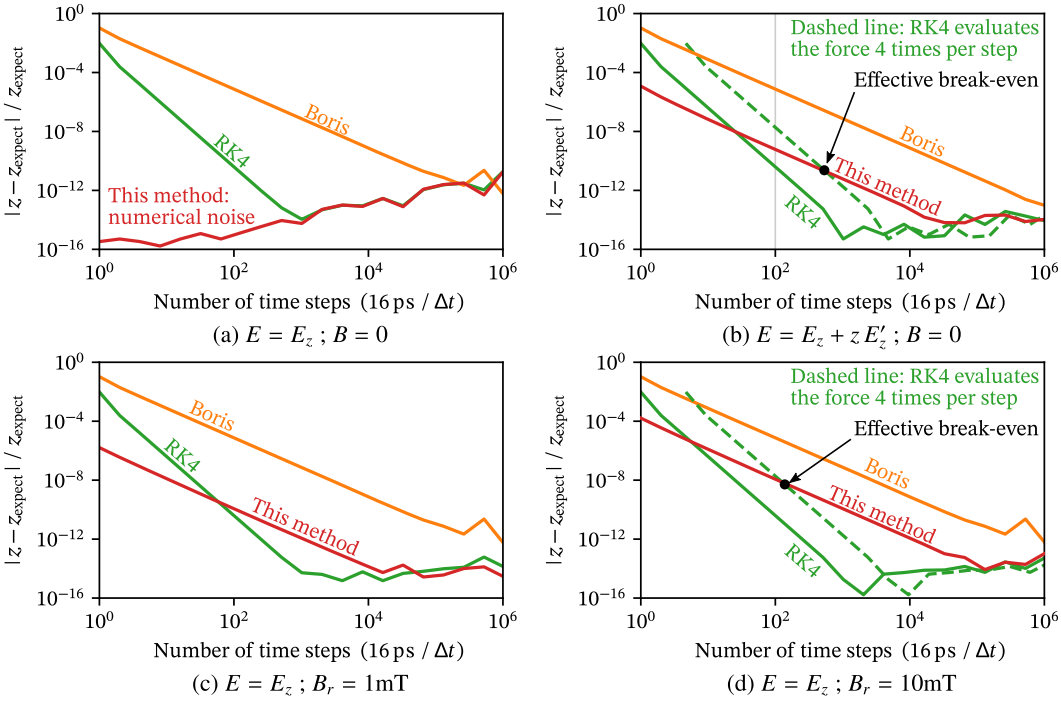

Fig. 4. Convergence of the particle final position in an electric field. Comparisons based on the number of force evaluations can be made by the dashed curve for RK4 and the curves of the other two methods.

3.1.1. Uniform axial electric field, zero magnetic field

The applied electric field is $\boldsymbol{E} = \hat{\boldsymbol{z}}\, E_z$. The strength of E_z is chosen so, that the relativity is significant. Initially, a particle starts at an arbitrary axial position $z = z_0$ and has an arbitrary initial $\boldsymbol{u}_0 = (u_{z0}, u_r, u_\theta)$, where the r and θ components of $\boldsymbol{u}_0$ are kept constant. The analytical solution of $z(t)$ is

$$z(t) = z_0 + c \int_0^t \frac{u_{z0} + \frac{q E_z}{m_0} t}{\sqrt{c^2 + (u_{z0} + \frac{q E_z}{m_0} t)^2 + u_r^2 + u_\theta^2}} \,\mathrm{d}\, t = z_0 + \frac{m_0\, c}{q\, E_z} \sqrt{c^2 + u_r^2 + u_\theta^2 + \left(\frac{q\, E_z}{m_0} t + u_{z_0}\right)^2} \Bigg|_0^t . \tag{13}$$

It is proven in appendix B, that the numerical solution $[z]_{n\,\Delta t}$ by the proposed method is identical to the analytical one:

$$[z]_{n\,\Delta t} = z(n\,\Delta t)\,, \tag{14}$$

where the number of steps n is a non-negative integer.

A test case is shown in Fig. 4(a). As expected, Boris method has the 2nd order convergence, while RK4 the 4th order. The proposed method has an exact solution, independent of the applied time step. One can see the growth of the numerical noise, when more time steps are going to be calculated.

3.1.2. Linearly increasing electric field, zero magnetic field

If the electric field is not constant, the proposed method is not exact anymore. To show the first order of perturbation, the axial electric field is set to have a constant gradient. The error of final position considering the following axial field

$$E(z) = -100\,\frac{\mathrm{kV}}{\mathrm{mm}} + \frac{z}{\mathrm{m}}\,\frac{\mathrm{kV}}{\mathrm{mm}} \quad , \quad B = 0 \tag{15a}$$

and a probe electron with initial parameters

$$z = 0 \quad , \quad u_z = -1 \times 10^8\,\frac{\mathrm{m}}{\mathrm{s}} \tag{15b}$$

for a total time of approximately 16 pico-seconds is shown in Fig. 4(b). The initial u_z has the order of magnitude comparable to the electrons in a gyrotron. It is negative, so that after a total deceleration and a re-acceleration, the final position is still around $z \approx 0$. All calculations are performed using 64 bit floating-point numbers, except the reference solution, which is calculated with RK4 using tiny steps and 128 bit precision numbers. A local average of the last converging points is taken as the reference solution. The initial velocities of the 2nd-order methods should be given at the time point $-1/2\Delta t$. They

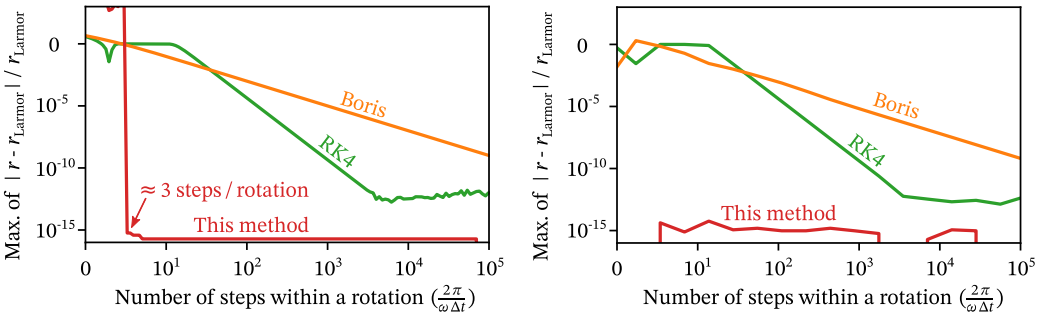

Fig. 5. Convergence of the centered large orbits for 1000 rotation cycles in a uniform magnetic field.

are obtained via backwards pushing the particle with the RK4 method for $1/2\Delta t$ time using small steps, even if the RK4 method is in principle not reversible.

From Fig. 4(b) one can see that the proposed method also has the 2nd-order convergence as Boris method, but the proposed one has a significantly better accuracy. For example, on the vertical line where the calculation is subdivided into 100 steps, the error of the proposed method is

$$\frac{7.489 \times 10^{-6}}{6.084 \times 10^{-10}} > 12000 \text{ times}$$

lower than Boris. This factor depends on the configuration. Especially if the gradient of electric field strength is small, the proposed method will always show a much lower error than Boris. In a high-order wildly non-uniform electric field, this advantage will disappear and the proposed method will perform similar to Boris method.

3.1.3. Uniform axial electric field, constant radial magnetic field

In this comparison, a constant B_r is considered in addition to the constant E_z. To fulfill $\nabla \cdot \boldsymbol{B} = 0$, there should be

$$B_z = -\frac{B_r z}{r} \approx 0 \quad \text{for } r \gg z\,, \tag{16a}$$

$$A_\theta = -B_r z\,. \tag{16b}$$

The other initial parameters are same as in section 3.1.2, except that there is no gradient in the electric field strength. A probe electron will start at a large radius, in order to minimize the influence of B_z, whose effects will be presented in the later sections.

Fig. 4(c) shows that the proposed method converges in the 2nd order as Boris in a weak B_r field, while its error level is significantly lower than Boris. If the perpendicular magnetic field is higher, the error level of the proposed method raises, as shown in Fig. 4(d). If the magnetic field is even higher, until $B_r \gg 1\,\mathrm{T}$ in this example, the error of the proposed method converges to the error of Boris.

3.2. Uniform axial magnetic field

The proposed method does not resolve the motion in θ direction. It may have advantages in the cases, when the θ component of the motion could cause deviations of trajectories. Two scenarios with the same uniform axial magnetic field are checked, in order to present the properties of the proposed method:

- the guiding center of the electron gyration is on the axis (centered large-orbit gyration),
- the guiding center radius is much larger than the Larmor radius (small-orbit gyration).

A non-centered large-orbit gyration is the intermediate case between the centered one and the small-orbit one, thus, it will not be presented here.

3.2.1. Large-orbit gyration

A uniform magnetic field of $B_z = 1\,\mathrm{T}$ is assumed. A probe electron is placed at $r = r_{\mathrm{Larmor}}$ with the initial velocity $u = u_\theta = 1 \times 10^8\,\mathrm{m/s}$, such that its rotation center is axis of the cylindrical coordinates. The $1/2\Delta t$ delay between position and velocity is taken into account for the 2nd-order methods.

Fig. 5 shows the convergence of the radius for the centered large-orbit gyrations. The maximum error within 1000 cyclotron cycles (a total angle of $1000 \times 2\pi$) is recorded and compared to each other. Fig. 5(a) only considers a B_z field, while Fig. 5(b) includes an additional radial electric field with the strength of $E_r = 1\,\mathrm{kV/cm}$. The latter case causes an $\boldsymbol{E} \times \boldsymbol{B}$

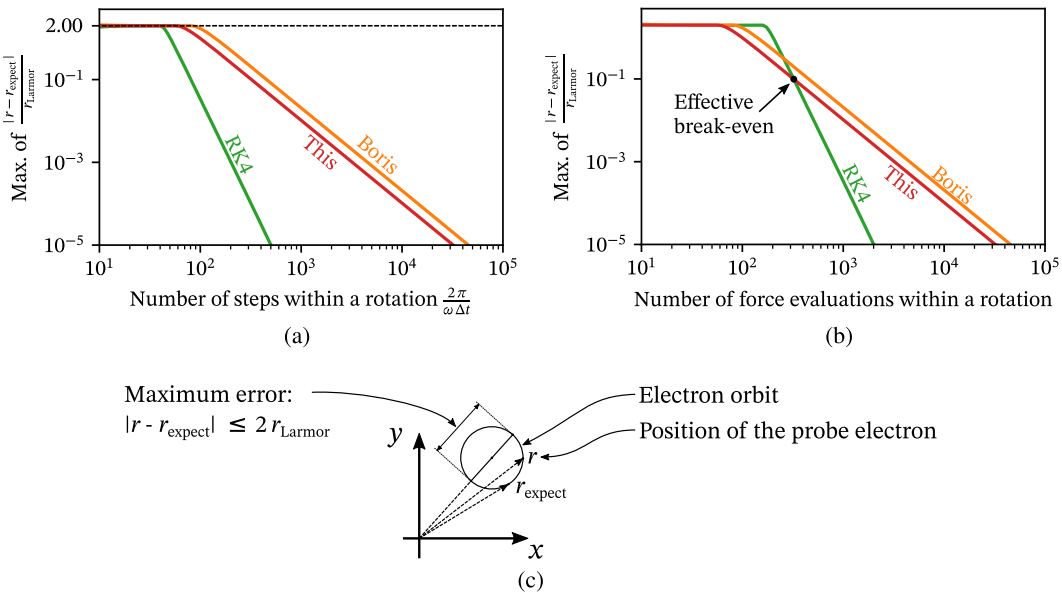

Fig. 6. Convergence of the small orbits for 1000 rotation cycles in a uniform magnetic field.

drift in θ direction. The proposed method yields exact solutions in both cases, since the net radial force exerted on the probe electron is zero.

3.2.2. Small-orbit gyration

The check of the small-orbit gyration considers the following parameters. The magnetic field is $B_z = 7\,\mathrm{T}$. A probe electron has $u = u_\theta = 1.8 \times 10^8\,\mathrm{m/s}$ (which corresponds to the kinetic energy of 90 keV) and its guiding center is at $r = 10\,\mathrm{mm}$ (typical in a fusion gyrotron). The probe electron will gyrate 1000 cycles.

Fig. 6(a) shows the maximum recorded errors of electron radial coordinate r normalized to the Larmor radius within the 1000 gyration cycles. At the beginning of the diagram, the accumulated phase error could become so large, that the simulated r and the expected r_{expect} could be on the opposite phases of a gyration. Therefore, the flat part of the curves has the value of two. This is visualized in Fig. 6(c).

As expected, Boris and the proposed method both converge at the 2nd order. However, the error of the proposed method is half of Boris. The comparison based on the number of force evaluations is shown in Fig. 6(b). RK4 only wins when the rotation cycle is resolved with tiny steps. Hence, the proposed method is also very worth to be considered in the small-orbit simulations.

3.3. Non-adiabatic magnetic field

The proposed method enforces the conservation of canonical angular momentum. This is generally not feasible with other methods. There are applications where the magnetic field is not adiabatic, such as cusp-guns [35] for large-orbit gyrotrons or for gyro-TWTs, non-adiabatic electron guns [36,37], and axisymmetric collectors [38–40] of vacuum tubes where the magnetic flux diverges intensively within a short distance. In these applications, the conservation of angular momentum is especially meaningful.

In this section, a magnetic cusp is taken for example. A cusp is where the magnetic field changes its sign. As the magnetic field vanishes at some point, the magnetic moment is no more a constant. However, the canonical angular momentum should still be conserved, as far as the system is axisymmetric. For instance, there is a negative magnetic field $B_z = -10\,\mathrm{mT}$ in the region of $z < 0$ and $B_z = 10\,\mathrm{mT}$ in the region of $z > 0$. In the interval around $z \approx 0$, the field still fulfills $\nabla \cdot \boldsymbol{B} = 0$ numerically. A very short cusp interval is chosen, because with such a short transition, the electron radius keeps almost unchanged before and after the cusp, so that one can have a coarse expectation of the correct result. (This case is explained e.g. in [41].) An electron from $z < 0$ travels with an initial velocity of $\boldsymbol{u} = \hat{\boldsymbol{z}}\, u_z$, where $u_z = 1 \times 10^8\,\mathrm{m/s}$, from the region $z < 0$ towards the cusp. The electron trajectories after the cusp are compared.

The electron trajectories for different methods are shown in Fig. 7(a). The proposed method has an almost unchanged radius after the transition, whereas the other reference methods introduce observable oscillations. The amplitude of oscillations from the other methods will converge to the proposed method, as the Δt becomes smaller. The difference to the initial radius as a parameter of the step number inside the cusp is shown in Fig. 7(b). The proposed method can handle the cusp with fewer steps than the other ones.

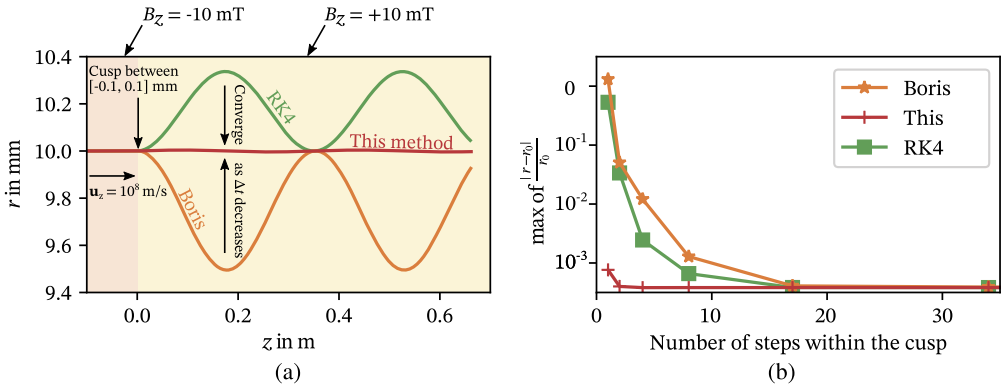

Fig. 7. Behaviors in a magnetic cusp.

4. Conclusion

A new method to calculate the particle trajectories in two-dimensional cylindrical coordinates considering the axisymmetry and static electric and magnetic fields is proposed. As an alternative to the classical Boris method, the proposed method shows better accuracy for the same time step in many cases. In particular, the trajectory is exact for the acceleration in a constant electric field (in absence of magnetic field), as well as for the centered large-orbit gyration in a magnetic field. Perturbations to these exact situations will have a much lower error level than the classical 2nd-order method. Besides, the proposed method evaluates v_θ directly from the canonical angular momentum, whose conservation is ensured by construction. Therefore, the method is expected to show its advantages especially in the simulation of non-adiabatic and cusp electron guns, non-adiabatic single and multiple stage collectors, where the results might be less sensitive to the simulation setups due to the enforced conservation. Showcases for these devices will be presented in the subsequent publications. For an outlook, the method can be modified to simulate the transient process in the static electric field, in the way that the total energy $\mathcal{E}_{\text{total}}$ has to be adjusted when the electric potential is updated.

CRediT authorship contribution statement

Chuanren Wu: Conceptualization, Methodology, Software, Writing - original draft. **Ioannis Gr. Pagonakis:** Methodology, Writing - review & editing. **Stefan Illy:** Writing - review & editing. **John Jelonnek:** Resources, Administration.

Declaration of competing interest

The authors declare that they have no known competing financial interests or personal relationships that could have appeared to influence the work reported in this paper.

Acknowledgements

We acknowledge support by the KIT-Publication Fund of the Karlsruhe Institute of Technology.

Appendix A. Another approach to derive the two-dimensional formulation

The formulation for the Lorentz factor

$$\gamma^2 = 1 + \frac{u_z^2 + u_r^2 + u_\theta^2}{c^2} \tag{A.1}$$

can be rearranged to

$$\frac{1}{2}u_z^2 + \frac{1}{2}u_r^2 = g\,, \tag{A.2}$$

where g is

$$g = \frac{1}{2}[c^2(\gamma^2 - 1) - u_\theta^2]\,. \tag{A.3}$$

For each particle, g depends only on the position, because both γ and u_θ depend only on the position. Hence, eq. (A.2) can be analogized to a two-dimensional conservative system if $B_\theta = 0$. Applying a total derivative of time on both sides of eq. (A.2) results in

$$\boldsymbol{u}\cdot\frac{\mathrm{d}\,\boldsymbol{u}}{\mathrm{d}\,t}=\boldsymbol{v}\cdot\nabla g\,. \tag{A.4}$$

Canceling $\boldsymbol{v}$ on both sides of eq. (A.4) yields the equation for advancing $\boldsymbol{u}$ in each time step:

$$\frac{\mathrm{d}\,\boldsymbol{u}}{\mathrm{d}\,t}=\frac{1}{\gamma}\nabla g\,, \tag{A.5}$$

where the gradient term is derived from eq. (A.3):

$$\nabla g=\left(0,\ \frac{u_\theta\,P_\theta}{m_0\,r^2}\right)+u_\theta\frac{q}{m_0}\nabla A_\theta+c^2\gamma\,\nabla\gamma\,. \tag{A.6}$$

$\nabla\gamma$ is given in eq. (9). Then, eq. (A.5) can be formulated only using potentials

$$\frac{\mathrm{d}\,\boldsymbol{u}}{\mathrm{d}\,t}=\left(0,\ \frac{v_\theta\,P_\theta}{m_0\,r^2}\right)+v_\theta\frac{q}{m_0}\nabla A_\theta-\frac{q}{m_0}\nabla\varphi\,, \tag{A.7}$$

where γ is a function only of the electric potential, see eq. (5b). An alternative formulation of eq. (A.7) is to use $\boldsymbol{E}$ and $\boldsymbol{B}$ instead of the potentials. For the derivation of this alternative form, one needs to expand $\boldsymbol{B}=\mathrm{curl}(\boldsymbol{A})$ in axisymmetric cylindrical coordinates, to obtain the components of the two-dimensional ∇A_θ:

$$\frac{\partial A_\theta}{\partial z}=-B_r\qquad\text{and}\qquad\frac{\partial A_\theta}{\partial r}=B_z-\frac{A_\theta}{r}=B_z-\frac{P_\theta}{q\,r^2}+\frac{m_0}{q\,r}\,u_\theta \tag{A.8}$$

eq. (A.7) is equivalent to

$$\frac{\mathrm{d}\,\boldsymbol{u}}{\mathrm{d}\,t}=\begin{pmatrix}\dfrac{q}{m_0}\,(E_z-v_\theta\,B_r)\\[2ex]\dfrac{q}{m_0}\,E_r+v_\theta\left(\dfrac{u_\theta}{r}+\dfrac{q}{m_0}\,B_z\right)\end{pmatrix} \tag{A.9}$$

This is another way to derive eq. (3).

Appendix B. Proof of eq. (14)

No matter whether the proposition of eq. (14) is true or not, the numerical value of u_z is exact:

$$[u_z]_{(n+\frac{1}{2})\,\Delta t}=u_z\Big((n+\frac{1}{2})\,\Delta t\Big)\,, \tag{B.1a}$$

which is the nominator of the integrand in eq. (13). If eq. (14) will turn to be true, then γ is also exact at time $n\,\Delta t$:

$$[\gamma]_{n\,\Delta t}=\gamma\,(n\,\Delta t)\,, \tag{B.1b}$$

since γ is derived from the position of the particle. The initial z position of the particle is an input (when $n=0$). For an inductive proof of eq. (14), it would be enough to show

$$[z]_{(n+1)\Delta t}-[z]_{n\Delta t}\overset{?}{=}z\Big((n+1)\Delta t\Big)-z\big(n\Delta t\big)\,. \tag{B.2}$$

The left-hand side of eq. (B.2) is

$$[z]_{(n+1)\Delta t}-[z]_{n\Delta t}=\Delta t\,\frac{[u_z]_{(n+\frac{1}{2})\,\Delta t}}{[\gamma]_{(n+\frac{1}{2})\,\Delta t}}\,, \tag{B.3}$$

where the numerical value of $[\gamma]$ is according to eq. (10)

$$[\gamma]_{(n+\frac{1}{2})\,\Delta t}=\frac{1}{2}\left([\gamma]_{n\,\Delta t}+\sqrt{[\gamma]^2_{n\,\Delta t}+\Delta t\,\frac{2\,q\,E_z}{m_0\,c^2}\,[u_z]_{(n+\frac{1}{2})\,\Delta t}}\right)=\frac{1}{2}\Big([\gamma]_{n\,\Delta t}+[\gamma]_{(n+1)\,\Delta t}\Big)\,, \tag{B.4}$$

which is actually the mid-position value, rather than the expected mid-time one. Inserting the numerical γ into eq. (B.3) results in

$$[z]_{(n+1)\Delta t}-[z]_{n\Delta t}=\Delta t\,\frac{[u_z]_{(n+1)\,\Delta t}+[u_z]_{n\,\Delta t}}{[\gamma]_{(n+1)\,\Delta t}+[\gamma]_{n\,\Delta t}}\,. \tag{B.5}$$

Multiplying $[u_z]_{(n+1)\,\Delta t}-[u_z]_{n\,\Delta t}=\Delta t\,q\,E_z/m_0$ to the fraction parts yields

$$[z]_{(n+1)\Delta t} - [z]_{n\Delta t} = \frac{m_0}{q\,E_z}\frac{[u_z]^2_{(n+1)\,\Delta t} - [u_z]^2_{n\,\Delta t}}{[\gamma]_{(n+1)\,\Delta t} + [\gamma]_{n\,\Delta t}} = \frac{m_0\,c^2}{q\,E_z}\frac{[\gamma]^2_{(n+1)\,\Delta t} - [\gamma]^2_{n\,\Delta t}}{[\gamma]_{(n+1)\,\Delta t} + [\gamma]_{n\,\Delta t}}\,, \tag{B.6}$$

which is identical to the analytical solution of the step distance on the right-hand side of eq. (B.2):

$$z\Big((n+1)\Delta t\Big) - z\big(n\Delta t\big) = \frac{m_0\,c^2}{q\,E_z}\left([\gamma]_{(n+1)\Delta t} - [\gamma]_{n\Delta t}\right). \tag{B.7}$$

Hence, the particle position in a (locally) uniform electric field can be exactly solved using the proposed method.

References

[1] J. Jelonnek, G. Aiello, F. Albajar, S. Alberti, K.A. Avramidis, A. Bertinetti, P.T. Brücker, A. Bruschi, I. Chelis, J. Dubray, F. Fanale, D. Fasel, T. Franke, G. Gantenbein, S. Garavaglia, J. Genoud, G. Granucci, J.-P. Hogge, S. Illy, Z.C. Ioannidis, J. Jin, H. Laqua, G.P. Latsas, A. Leggieri, F. Legrand, R. Marchesin, A. Marek, B. Marlétaz, M. Obermaier, I.G. Pagonakis, D.V. Peponis, S. Ruess, T. Ruess, T. Rzesnicki, P. Sanchez, L. Savoldi, T. Scherer, D. Strauss, P. Thouvenin, M. Thumm, I. Tigelis, M.-Q. Tran, F. Wilde, C. Wu, A. Zisis, From W7-X towards ITER and beyond: 2019 status on EU fusion gyrotron developments, in: 20th International Vacuum Electronics Conference, 2019.

[2] A. Abragam, M. Goldman, Principles of dynamic nuclear polarisation, Rep. Prog. Phys. 41 (3) (1978) 395–467, https://doi.org/10.1088/0034-4885/41/3/002.

[3] M. Blank, K. Felch, B.G. James, P. Borchard, P. Cahalan, T.S. Chu, H. Jory, B.G. Danly, B. Levush, J.P. Calame, K.T. Nguyen, D.E. Pershing, Development and demonstration of high-average power w-band gyro-amplifiers for radar applications, IEEE Trans. Plasma Sci. 30 (3) (2002) 865–875, https://doi.org/10.1109/tps.2002.801658.

[4] K.A. Avramides, I.G. Pagonakis, C.T. Iatrou, J.L. Vomvoridis, EURIDICE: a code-package for gyrotron interaction simulations and cavity design, in: European Physical Journal Web of Conferences, vol. 32, 2012, p. 04016.

[5] S. Alberti, T.M. Tran, K.A. Avramides, F. Li, J.-P. Hogge, Gyrotron parasitic-effects studies using the time-dependent self-consistent monomode code TWANG, in: International Conference on Infrared, Millimeter, and Terahertz Waves, IEEE, 2011.

[6] H. Busch, Berechnung der Bahn von Kathodenstrahlen im axialsymmetrischen elektromagnetischen Felde, Ann. Phys. 386 (25) (1926) 974–993, https://doi.org/10.1002/andp.19263862507.

[7] W.B. Herrmannsfeldt, Electron trajectory program, Tech. Rep. SLAC 226, Stanford Linear Accelerator Center, Stanford, CA, 94305, 11 1979.

[8] E. Borie, C. Gruber, T. Westermann, Calculation of MIG guns for gyrotrons using the BFCPIC code, Int. J. Electron. 78 (4) (1995) 789–807, https://doi.org/10.1080/00207219508926210.

[9] T.M. Tran, D.R. Whaley, S. Merazzi, R. Gruber DAPHNE, A 2D axisymmetric electron gun simulation code, in: Proc. 6th Joint EPS-APS International Conference on Physics Computing, Lugano, Switzerland, 1994, pp. 491–494.

[10] C.J. Edgcombe, Sources of velocity spread in electron beams from magnetron injection guns, Int. J. Infrared Millim. Waves 16 (1) (1995) 83–97, https://doi.org/10.1007/bf02085848.

[11] V.K. Lygin, V.N. Manuilov, S.E. Tsimring, Effective code for numerical simulation of the helical relativistic electron beams, in: 11th International Conference on High-Power Particle Beams, vol. 1, 1996, pp. 385–388.

[12] S. Illy, J. Zhang, J. Jelonnek, Gyrotron electron gun and collector simulation with the ESRAY beam optics code, in: International Vacuum Electronics Conference (IVEC), IEEE, 2015, pp. 1–2.

[13] J.G. Pagonakis, J.L. Vomvoridis, The self-consistent 3D trajectory electrostatic code ARIADNE for gyrotron beam tunnel simulation, in: Proc. Infrared and Millimeter Waves Conf., 2004, pp. 657–658.

[14] J.P. Boris, Relativistic plasma simulation-optimization of a hybrid code, in: Proceedings of the Fourth Conference on Numerical Simulation of Plasmas, Naval Research Laboratory, 1970, pp. 3–67.

[15] R.I. McLachlan, M. Perlmutter, Energy drift in reversible time integration, J. Phys. A, Math. Gen. 37 (45) (2004) L593–L598, https://doi.org/10.1088/0305-4470/37/45/l01.

[16] H. Qin, S. Zhang, J. Xiao, J. Liu, Y. Sun, W.M. Tang, Why is Boris algorithm so good?, Phys. Plasmas 20 (8) (2013) 084503, https://doi.org/10.1063/1.4818428.

[17] C.K. Birdsall, A.B. Langdon, Plasma Physics via Computer Simulation, IOP Publishing Ltd, 1991.

[18] P.H. Stoltz, J.R. Cary, G. Penn, J. Wurtele, Efficiency of a Boris-like integration scheme with spatial stepping, Phys. Rev. Spec. Top., Accel. Beams 5 (9) (2002), https://doi.org/10.1103/physrevstab.5.094001.

[19] G. Penn, P.H. Stoltz, J.R. Cary, J. Wurtele, Boris push with spatial stepping, J. Phys. G, Nucl. Part. Phys. 29 (8) (2003) 1719–1722, https://doi.org/10.1088/0954-3899/29/8/337.

[20] B. Ripperda, F. Bacchini, J. Teunissen, C. Xia, O. Porth, L. Sironi, G. Lapenta, R. Keppens, A comprehensive comparison of relativistic particle integrators, Astrophys. J. Suppl. Ser. 235 (1) (2018) 21, https://doi.org/10.3847/1538-4365/aab114.

[21] J.-L. Vay, Simulation of beams or plasmas crossing at relativistic velocity, Phys. Plasmas 15 (5) (2008) 056701, https://doi.org/10.1063/1.2837054.

[22] S. Zenitani, T. Umeda, On the Boris solver in particle-in-cell simulation, Phys. Plasmas 25 (11) (2018) 112110, https://doi.org/10.1063/1.5051077.

[23] A.V. Higuera, J.R. Cary, Structure-preserving second-order integration of relativistic charged particle trajectories in electromagnetic fields, Phys. Plasmas 24 (5) (2017) 052104, https://doi.org/10.1063/1.4979989.

[24] T. Umeda, A three-step Boris integrator for Lorentz force equation of charged particles, Comput. Phys. Commun. 228 (2018) 1–4, https://doi.org/10.1016/j.cpc.2018.03.019.

[25] S.E. Parker, C.K. Birdsall, Numerical error in electron orbits with large $\omega_{ce}\,\Delta t$, J. Comput. Phys. 97 (1) (1991) 91–102, https://doi.org/10.1016/0021-9991(91)90040-R.

[26] S. Zenitani, T.N. Kato, Multiple Boris integrators for particle-in-cell simulation, Comput. Phys. Commun. 247 (2020) 106954, https://doi.org/10.1016/j.cpc.2019.106954.

[27] A.V. Arefiev, G.E. Cochran, D.W. Schumacher, A.P.L. Robinson, G. Chen, Temporal resolution criterion for correctly simulating relativistic electron motion in a high-intensity laser field, Phys. Plasmas 22 (1) (2015) 013103, https://doi.org/10.1063/1.4905523.

[28] G.L. Delzanno, E. Camporeale, On particle movers in cylindrical geometry for particle-in-cell simulations, J. Comput. Phys. 253 (2013) 259–277, https://doi.org/10.1016/j.jcp.2013.07.007.

[29] J.M. Wallace, J.U. Brackbill, D.W. Forslund, An implicit moment electromagnetic plasma simulation in cylindrical coordinates, J. Comput. Phys. 63 (2) (1986) 434–457, https://doi.org/10.1016/0021-9991(86)90203-2.

[30] H. Li, Q. Hong, An efficient energy-preserving algorithm for the Lorentz force system, Appl. Math. Comput. 358 (2019) 161–168, https://doi.org/10.1016/j.amc.2019.04.035.

[31] M. Reiser, Theory and Design of Charged Particle Beams, Wiley-VCH, 2008.
[32] T. Rzesnicki, F. Albajar, S. Alberti, K.A. Avramidis, W. Bin, T. Bonicelli, F. Braunmueller, A. Bruschi, J. Chelis, P.-E. Frigot, G. Gantenbein, V. Hermann, J.-P. Hogge, S. Illy, Z.C. Ioannidis, J. Jin, J. Jelonnek, W. Kasparek, G.P. Latsas, C. Lechte, M. Lontano, T. Kobarg, I.G. Pagonakis, Y. Rozier, C. Schlatter, M. Schmid, I.G. Tigelis, M. Thumm, M.Q. Tran, J.L. Vomvoridis, A. Zisis, Experimental verification of the European 1-MW, 170-GHz industrial CW prototype gyrotron for ITER, Fusion Eng. Des. 123 (2017) 490–494, https://doi.org/10.1016/j.fusengdes.2017.02.021.
[33] G. Schmidt, Physics of High Temperature Plasmas, Academic Press, 1979.
[34] P.V. Krivosheev, V.K. Lygin, V.N. Manuilov, S.E. Tsimring, Numerical simulation models of forming systems of intense gyrotron helical electron beams, Int. J. Infrared Millim. Waves 22 (8) (2001) 1119–1145, https://doi.org/10.1023/A:1015006230396.
[35] C.R. Donaldson, W. He, A.W. Cross, F. Li, A.D.R. Phelps, L. Zhang, K. Ronald, C.W. Robertson, C.G. Whyte, A.R. Young, A cusp electron gun for millimeter wave gyrodevices, Appl. Phys. Lett. 96 (14) (2010) 141501, https://doi.org/10.1063/1.3374888.
[36] B. Piosczyk, Non-adiabatic electron gun for gyrotrons, Int. J. Electron. 67 (3) (1989) 447–456, https://doi.org/10.1080/00207218908921099.
[37] A.L. Goldenberg, M.Y. Glyavin, K.A. Leshcheva, V.N. Manuilov, Nonadiabatic electron-optical system of a technological gyrotron, Radiophys. Quantum Electron. 60 (5) (2017) 395–400, https://doi.org/10.1007/s11141-017-9808-9.
[38] A. Singh, V.L. Granatstein, G. Hazel, G. Saraph, J.M. Cooperstein, T. Hargreaves, A depressed collector system for a quasi-optical gyrotron with precisely controlled magnetic flux lines, Int. J. Infrared Millim. Waves 12 (1991) 323–334, https://doi.org/10.1007/BF01009406.
[39] C. Wu, I.G. Pagonakis, S. Illy, M. Thumm, G. Gantenbein, J. Jelonnek, Preliminary studies on multistage depressed collectors for fusion gyrotrons, in: 10th German Microwave Conference, Bochum, Germany, 2016.
[40] M.V. Morozkin, M.Y. Glyavin, V.N. Manuilov, I.V. Zotova, M.D. Proyavin, Collector system of a gyrotron with magnetically shielded solenoid, EPJ Web Conf. 149 (2017) 04043, https://doi.org/10.1051/epjconf/201714904043.
[41] Tsimring, Electron Beams, John Wiley & Sons, 2006.